5. Vaidyanathan G, Zalutsky MR. No-carrier-added synthesis of *meta*-[^{131}I]iodobenzylguanidine. *Appl Radiat Isot* 1993;44:621–628.
6. Vaidyanathan G, Zalutsky MR. No-carrier-added [^{123}I]MIBG: synthesis and preliminary evaluation. *Nucl Med Biol* 1995;22:61–64.
7. Vaidyanathan G, Zalutsky MR. 1-(*m*-[^{211}At]Astatobenzyl)guanidine: synthesis via astato demetalation and preliminary in vitro and in vivo evaluation. *Bioconj Chem* 1992;3:499–503.
8. Vaidyanathan G, Strickland DK, Zalutsky MR. *Meta*-[^{211}At]astatobenzylguanidine: further evaluation of a potential therapeutic agent. *Int J Cancer* 1994;57:908–913.
9. Vaidyanathan G, Affleck DJ, Zalutsky MR. 4-[^{18}F]Fluoro-3-iodobenzylguanidine: a potential MIBG analog for positron emission tomography. *J Med Chem* 1994;37:3655–3662.
10. Vaidyanathan G, Affleck DJ, Zalutsky MR. Validation of 4-[^{18}F]fluoro-3-iodobenzylguanidine as a potential PET analog of MIBG. *J Nucl Med* 1995;36:644–650.
11. Ott RJ, Tait D, Flower MA, Babich JW, Lambrecht RM. Treatment planning for ^{131}I-MIBG radiotherapy of neural crest tumours using ^{124}I-MIBG positron emission. *Br J Radiol* 1992;65:787–791.
12. Loc'h C, Mardon K, Valette H, Brutesco C, Merlet P, Syrota A, Maziere B. Preparation and pharmacological characterization of [^{76}Br]-*meta*-bromobenzylguanidine ([^{76}Br]MBBG). *Nucl Med Biol* 1994;21:49–55.
13. Valette H, Loc'h C, Mardon K, et al. Bromine-76-metabromobenzylguanidine: a PET radiotracer for mapping sympathetic nerves of the heart. *J Nucl Med* 1993;34:1739–1744.
14. Garg PK, Garg S, Zalutsky MR. Synthesis and preliminary evaluation of *para*- and *meta*-[^{18}F]fluorobenzylguanidine. *Nucl Med Biol* 1994;21:97–103.
15. Shulkin BL, Shapiro B, Francis I, Door R, Shew S-W, Sisson JC. Primary extra-adrenal pheochromocytoma positive ^{123}I MIBG imaging with negative ^{131}I MIBG imaging. *Clin Nucl Med* 1986;11:851–854.
16. Vaidyanathan G, Affleck DJ, Zalutsky MR. No-carrier-added 4-fluoro-3-[^{131}I]iodobenzylguanidine and 3-[^{211}At]astato-4-fluorobenzylguanidine. *Bioconj Chem* 1996;7:102–107.
17. Biedler JL, Helson L, Spengler BA. Morphology and growth, tumorigenicity and cytogenetics of human neuroblastoma cells in continuous culture. *Cancer Res* 1973;33:2643–2652.
18. Smets LA, Loesberg C, Janssen M, Metwally EA, Huiskamp R. Active uptake and extravesicular storage of *m*-iodobenzylguanidine in human neuroblastoma SK-N-SH cells. *Cancer Res* 1989;49:2941–2944.
19. Buck J, Bruchelt G, Girgert R, Treuner J, Niethammer D. Specific uptake of m-[^{125}I]iodobenzylguanidine in the human neuroblastoma cell line SK-N-SH. *Cancer Res* 1985;45:6366–6370.
20. Smets LA, Janssen M, Rutgers M, Ritzen K, Buitenhuis C. Pharmacokinetics and intracellular distribution of the tumor-targeted radiopharmaceutical *m*-iodo-benzylguanidine in SK-N-SH neuroblastoma and PC-12 pheochromocytoma cells. *Int J Cancer* 1991;48:609–615.
21. Guerreau D, Thedrez P, Fritsch P, et al. In vitro therapeutic targeting of neuroblastoma using ^{125}I-labeled meta-iodobenzylguanidine. *Int J Cancer* 1990;45:1164–1168.
22. Mairs RJ, Gaze MN, Barret A. The uptake and retention of metaiodobenzylguanidine by the neuroblastoma cell line NB1-G. *Br J Cancer* 1991;64:293–295.
23. Lashford LS, Hancock JP, Kemshead JT. *Meta*-iodobenzylguanidine (MIBG) uptake and storage in the human neuroblastoma cell line SK-N-BE(2C). *Int J Cancer* 1991;47:105–109.
24. Jaques S, Tobes MC, Sisson JC. Sodium dependency of uptake of norepinephrine and m-iodobenzylguanidine into cultured human pheochromocytoma cells: evidence for uptake-one. *Cancer Res* 1987;47:3920–3928.
25. Smets LA, Janssen M, Metwally E, Loesberg C. Extragranular storage of the neuron blocking agent meta-iodobenzylguanidine (MIBG) in human neuroblastoma cells. *Biochem Pharmacol* 1990;39:1959–1964.
26. Smets LA, Bout B, Wisse J. Cytotoxic and antitumor effects of the norepinephrine analog meta-iodo-benzylguanidine (MIBG). *Cancer Chemother Pharmacol* 1988;21:9–13.
27. Servidei T, Iavarone A, Lasorella A, Mastrangelo S, Riccardi R. Release mechanisms of [^{125}I]metaiodobenzylguanidine in neuroblastoma cells: evidence of a carrier-mediated efflux. *Eur J Cancer* 1995;31A:591–595.
28. Mangner TJ, Tobes MC, Wieland DW, Sisson JC, Shapiro B. Metabolism of iodine-131-metaiodobenzylguanidine in patients with metastatic pheochromocytoma. *J Nucl Med* 1986;27:37–44.
29. Zalutsky MR, Narula AS. A method for the radiohalogenation of proteins resulting in decreased thyroid uptake of radioiodine. *Appl Radiat Isot* 1987;38:1051–1055.

Weighted Summation of Oxygen-15-Water PET Data to Increase Signal-to-Noise Ratio for Activation Studies

Jesper L.R. Andersson and Harald Schneider
Uppsala University PET Centre, Department of Radiation Sciences, Subfemtomole Biorecognition Project, Uppsala, Sweden

Data with the highest possible signal-to-noise (S/N) ratios are desirable when performing nonquantitative perturbation studies with PET and ^{15}O-water. To achieve this, protocols have been suggested in which the stimulus is switched off before the washout phase. An alternative strategy is suggested for cases in which the stimulus is not easily discontinued. **Methods:** For a given subject, a theoretical signal curve is created by simulating tissue time-activity curves for baseline and activated states and their subtraction. The curve is created from a typical arterial curve, and values for delay and flow are estimated for that subject. When summing the activity data before image reconstruction, the values from the signal curve are used as weights. Thus, data with high information content regarding changes in blood flow are given a large weight, and data with less information are given a smaller weight. The method is examined by simulations, and the results are validated by application to data from 10 individuals from an activation study. **Results:** Simulations show that the S/N ratio peaks for a given summation time and then decline for longer times when performing a straight summation of data. This time is not constant and varies both with the whole brain flow level and the magnitude of the activation. When using weighted summation on the other hand, the S/N ratio approaches asymptotically its optimal value. The optimal S/N value for weighted summation is 5%–10% higher than the peak value obtained with straight summation. The results are confirmed by the experimental data, indicating a shift in optimal summation time from 60–100 sec and an increase by 6% in the S/N ratio for weighted compared to straight summation. **Conclusion:** The method presented in this paper offers a way to significantly increase the S/N ratio in ^{15}O-water perturbation studies without increasing invasiveness or complicating the experimental protocol.

Key Words: PET; activation study; signal-to-noise ratio

J Nucl Med 1997; 38:334–340

PET studies with ^{15}O-water are a powerful tool to study altered cerebral blood flow as a consequence of physiological activation (*1*), pharmacological perturbation (*2*) or physiological or pathophysiological state (*3*). The methodology is based on the detection of regional differences between two or more scans in which the subject is in different states. Absolute quantification of the magnitude of change requires arterial sampling (*4,5*) and is therefore often sacrificed to enable simpler and less invasive procedures (*6*). There has been, however, some controversy about which integration time to use for optimal S/N ratios with respect to changes in blood flow. Time suggestions range from 60 to 100 sec after the arrival of the bolus to the brain (*7,8*). While the noise level tends to decrease with increased integration time, the signal will peak

Received Apr. 24, 1995; revision accepted Jan. 28, 1996.
For correspondence or reprints contact: Jesper Andersson, PhD, Uppsala University PET Centre, S-751 85 Uppsala, Sweden.

relatively soon after injection due to differential washout as well as uptake. This has been successfully addressed in activation studies by turning off the stimulation after an appropriate time, thus avoiding differential washout (*9*). The baseline study was also switched (*10*). Both the single-switched and the double-switched protocols have been shown to yield significant improvements in S/N ratios compared to nonswitched techniques (*9,10*), although the latter would seem impractical in many activation protocols considering the resulting specificity of the baseline study.

There is, however, still a family of studies for which a rapid switch of the parameter influencing the blood flow is not possible to obtain. Examples of such studies would be pharmacological perturbations of rCBF (*2*), rCBF studies during wakefulness and sleep, rCBF studies of migraine patients during and between headache attacks (*11*) and rCBF in bipolar patients during positive and negative symptoms. These types of studies has previously been hard to analyze by subtraction analysis due to the difficulty of obtaining accurate repositioning of the subjects, but recent advances in registration methods (*12,13*) have made it possible to adopt the same statistical analysis methods that have been used for activation studies (*14,15*). Thus, for these types of studies the question of integration time is still vital to obtain data with an optimal S/N ratio.

In this article, we will show that the integration time yielding optimal S/N ratios is not constant but depends on the magnitude of both absolute baseline flow and flow change. A method for weighted summation, yielding enhanced S/N ratios independent of the aforementioned parameters, is suggested.

MATERIALS AND METHODS

Theory

Kinetics of $H_2{}^{15}O$ in Brain Tissue. The equation used to describe the kinetics of water in brain tissue is (*4,16,17*):

$$C(t) = f\tau g(t + \Delta t) + f\left(1 - \tau\frac{f}{\lambda}\right)\int_0^t g(s + \Delta t)e^{-f/\lambda\,(t-s)}ds\,, \quad \text{Eq. 1}$$

in which C denotes decay-corrected activity concentration in the brain, g denotes decay-corrected arterial activity concentration as measured by an external device, f denotes flow, λ denotes distribution volume, Δt denotes delay between tracer arrival to the brain and tracer arrival to the external blood measurement device and τ denotes dispersion introduced by the external blood measurement.

Rationale. After a bolus injection of $H_2{}^{15}O$, the activity concentration in the brain rapidly increases to a level determined by the local blood flow. For areas with a high blood flow, the activity will peak at a higher level than for areas with low flow. After the peak, the tracer will start to wash out of the brain, the washout rate being greater in high flow than low flow areas. Hence, the magnitude of the difference between high and low flow areas will start to diminish soon after the activity has peaked. Naturally, the same effect applies when comparing the same area at two different flow levels, as in activation studies. Therefore, the maximum signal would be obtained by using data from a very short time centered around the peak of activity in the brain. It is, however, the S/N ratio that should be maximized, and the noise level decreases when increasing the summation time. It has been shown that the S/N ratio peaks for a given summation time and then starts to decrease (*7,10*). Thus, the strategy that is commonly used is to sum data from the time of tracer arrival to the brain and approximately 60–80 sec forward. When simulating and measuring the difference in activity concentration it is found that a difference between activated and baseline state persists for approximately 180 sec, although it becomes smaller (*10*). This implies there is still valuable information at later times that is discarded when summing for only 60–80 sec.

The aim of this work was to examine whether this information may be extracted by weighting the data so that data collected at earlier times will be given a higher weight in the summation compared to data collected at later times. The exact weights are calculated by creating simulated baseline and activated time-activity curves, using parameters relevant for each subject. A signal curve is created by subtracting the baseline from the activated curve, and the weights are calculated from the signal curve. The notion to use a weighting rather than a straight summation of ^{15}O-water data is not new and has been utilized previously to obtain quantitative flow values with close to optimal S/N ratios (*18*).

Simulations

Arterial Input Function. Blood curves with a "typical" appearance obtained by an automatic blood sampler (*19*) with a sampling density of 1 Hz in four different individuals (not participating in the present study) were averaged to create a representative mean input function. A VAX-station 4000/60 running VMS was used for all calculations presented in this article

Simulation of Signal. Let $C(t;(g,f,\lambda,\Delta t,\tau))$ denote tissue activity over time as evaluated with Equation 1. A non-decay-corrected tissue curve for a "typical" gray matter pixel may then be described as:

$$\sum_{i=0}^{2} w_i C(t; (g, f_i, \lambda_i, \Delta t, \tau)) \cdot e^{-(\ln 2/T_{1/2})t}, \quad \text{Eq. 2}$$

in which w_i denotes the relative abundance, f_i denotes the flow and λ_i denotes the distribution volume of the i:th tissue type. The two tissue types used were gray and white matter, and the proportions for a "typical" gray matter pixel were assumed to be 30% white and 70% gray matter. Values for λ were 0.86 and 1.03 ml/ml for white and gray matter, respectively (*20*). The values for *f* were varied to simulate different flow levels but for the baseline curves they were always varied together so that the ratio between gray and white matter flow was 4:1. When generating a tissue curve for the activated state, the flow value for the gray matter proportion was multiplied by 1.0 + 0.01X to simulate an X% activation, while the flow of the white matter proportion was kept constant. The signal curve was obtained by subtracting the baseline curve from the curve for the activated state.

Noise Simulation. A whole-brain tissue curve was generated by assuming a 50:50 distribution of white and gray matter. The noise was assumed to be proportional to the square root of the whole brain curve after its multiplication by two. This estimate of noise is valid only if the noise is assumed to be stationary (*18*), an assumption that has empirical support (*15*).

Signal-to-Noise Ratio. A signal-to-noise ratio curve was obtained by dividing the signal by the noise for every time t. An integral signal-to-noise ratio curve was obtained by first integrating the signal curve and the whole-brain curve from time zero to time t. An estimate of the noise was obtained by taking the square root of the whole brain integral multiplied by two. Finally, the integral of the signal curve was divided by the noise estimate. Note that the integral signal-to-noise ratio curve does not equal the integral of the signal-to-noise ratio curve. It is the integral signal-to-noise ratio that is usually implied when discussing signal-to-noise ratio in this context, and it is therefore referred to as S/N ratio throughout this article. By varying the flow and activation levels and by evaluating

the S/N ratio curve with a time resolution of 1 sec, the optimal integration time for the different flow and activation levels could be obtained.

Weighted Summation. To simulate the effect of weighted summation a weighted integration of the signal curve was performed using the signal-to-noise ratio curve as weight function. When integrating the whole-brain curve, the square of the signal-to-noise ratio curve was used as a weight function. An S/N curve was again created by dividing the weighted integral of the signal curve by the noise estimate from the weighted whole-brain curve. Again, the flow and activation levels were varied to examine the influence of these parameters.

Experiments

Scanning Protocol. Ten healthy male volunteers (aged 22–31 yr) each underwent five bolus injections of 10–15 MBq/kg body weight of $H_2{}^{15}O$ while performing different tasks. Prior to emission scanning, they had been positioned in the scanner and immobilized in a headholder with a fast-hardening foam, after which a transmission scan was obtained, yielding 50–150 counts per projection through the central parts of the brain. The first scan was performed with the subject resting in the scanner with his eyes closed, and the second while the subject was tracking a predrawn zigzag line with a pen on a paper. Compared to the baseline, the second scan was expected to activate mainly visual and motor areas. Data from the subsequent activations are not used in this study. Thus, the paradigms are not described in this article. Each emission scan was started when the bolus was injected and consisted of 15 frames of 10 sec duration. Throughout the examination the total counting rate for each slice was collected with a sampling density of 1 Hz. The studies were performed on a GE PC2048B scanner producing 15 slices with 6.5-mm slice spacing and 6-mm axial and transaxial FWHM (*21*).

Estimation of Gray Matter Weighted Whole-Brain Blood Flow. The same mean input function used for the simulations was used in Equation 1 when fitting it to the total counting rate curve averaged over slices seven, eight and nine. In the fitting procedure, the dispersion was fixed to 10 sec and the other parameters were allowed to vary freely. Because it is not possible to calibrate the counting rate curve, the fitted value for f was not used. Instead, the estimate of f/λ (i.e., the washout rate constant) was multiplied with an assumed value for λ of 0.90 ml/ml, yielding an estimate of f. This type of analysis can be viewed as washout analysis, comparable to the ^{133}Xe technique (*22*), in which the presence of recirculating tracer is compensated for by the use of a measured input function. For each subject, the whole-brain blood flow was averaged over all five injections.

Evaluation of Weights. The estimated whole-brain blood flow averaged over all five scans was used in Equation 1, together with the mean input function, to create a theoretical baseline time-activity curve for each subject. A theoretical activated time-activity curve was obtained by multiplying the estimated flow by 1.20, thus simulating an activation of 20% magnitude. By subtracting the baseline from the activated time-activity curve, a theoretical signal curve was obtained. The signal curve was adjusted in time for each injection using the delay time obtained from the fitting procedure. To yield the weight for each frame, the signal curve was integrated within the time span of each frame. Finally, the weights were normalized so that the average weight was 1.0.

Summation and Reconstruction of Data. Projection data for the two first scans for each subject were summed to yield datasets representing the activity concentration for the first 40, 60, 80, 100 and 120 sec after arrival of the bolus to the brain. The time of bolus arrival to the brain was determined by backwards extrapolation of a line drawn through two points representing 20% and 50% of the peak activity in the counting rate curve for the three middle slices (*23*). Both straight summation (all weights equal to 1.0) and weighted summation were performed for each summation time. Because the singles were used to estimate randoms and deadtime, it was also important to know how they were summed. As a first approximation, we chose to weight the singles data when summing these. The summed frames were reconstructed to a 128 × 128 mm matrix, correcting for dead time, scatter (*24*) and attenuation.

Creation of Subtraction Images. Any movements between the two injections were compensated for by software realignment of the second examination to the first (*13*). In no subject had there been a movement exceeding 3 mm between the two scans, hence the attenuation correction was considered to be adequate (*25*). Global changes between the two examinations were normalized (*6*). Images were filtered with a 10-mm FWHM Gaussian filter and a pixel by pixel subtraction was performed.

Signal and Noise Measurement. Two circular regions of interest (ROIs) with a 15-mm radius were created in two subsequent slices, centered around the activation of the calcarine cortex as visualized in the subtraction images. The average pixel value within these ROIs was used as a measure of the signal. Large ROIs representing mainly the cortex of the frontal parts of the brain were drawn on freehand in several consecutive slices in the baseline images. When performing the group analysis of the data, no significant or close to significant activation was found in this part of the brain [maximum z-score 2.39 in a volume approximately corresponding to 100 resolution elements (*15*)]. Thus, it can be argued that the s.d. between the pixels within these ROIs represents a measure of the noise.

RESULTS

Simulations

The simulations confirmed that the S/N ratio peaks for a given summation time and then starts to decline when performing a straight summation. Examples of brain-activity curves, signal curves, signal-to-noise ratio curves and S/N ratio curves obtained from the simulations are shown in Figure 1. It is evident from panels 2 and 3 in Figure 1 that although the majority of the information lies within the first 60 sec after injection, there is still a positive signal for times under 180 sec.

Optimal summation time (the time for which the S/N ratio curve peaks) as a function of baseline flow level and activation magnitude is shown in Figure 2. A strong dependence on the baseline flow level is evident from the left part of Figure 2, indicating there is no one optimal summation time. Indeed, when considering an activation of 30% magnitude, optimal S/N ratio for a subject with a low global flow (35 ml/(min · 100 ml)) would be obtained for a summation time of 100 sec, whereas it would be achieved for a summation time of 65 sec in a subject with high global flow (55 ml/(min · 100 ml)). For an average subject, with a global flow of approximately 45 ml/(min · 100 ml), a summation time of 75–80 sec would seem appropriate. A considerably smaller dependence on the activation level is demonstrated by the right part of Figure 2.

Conversely, when performing a weighted summation, the S/N ratio increases and plateaus at a level slightly higher than the peak value obtained for straight summation. This behavior is demonstrated on the left side of Figure 4, which compares the S/N ratio curves for straight and weighted summation. The same effect was observed for all examined combinations of flow and activation level, and the plateau was always 5%–10% higher than the peak value for straight summation.

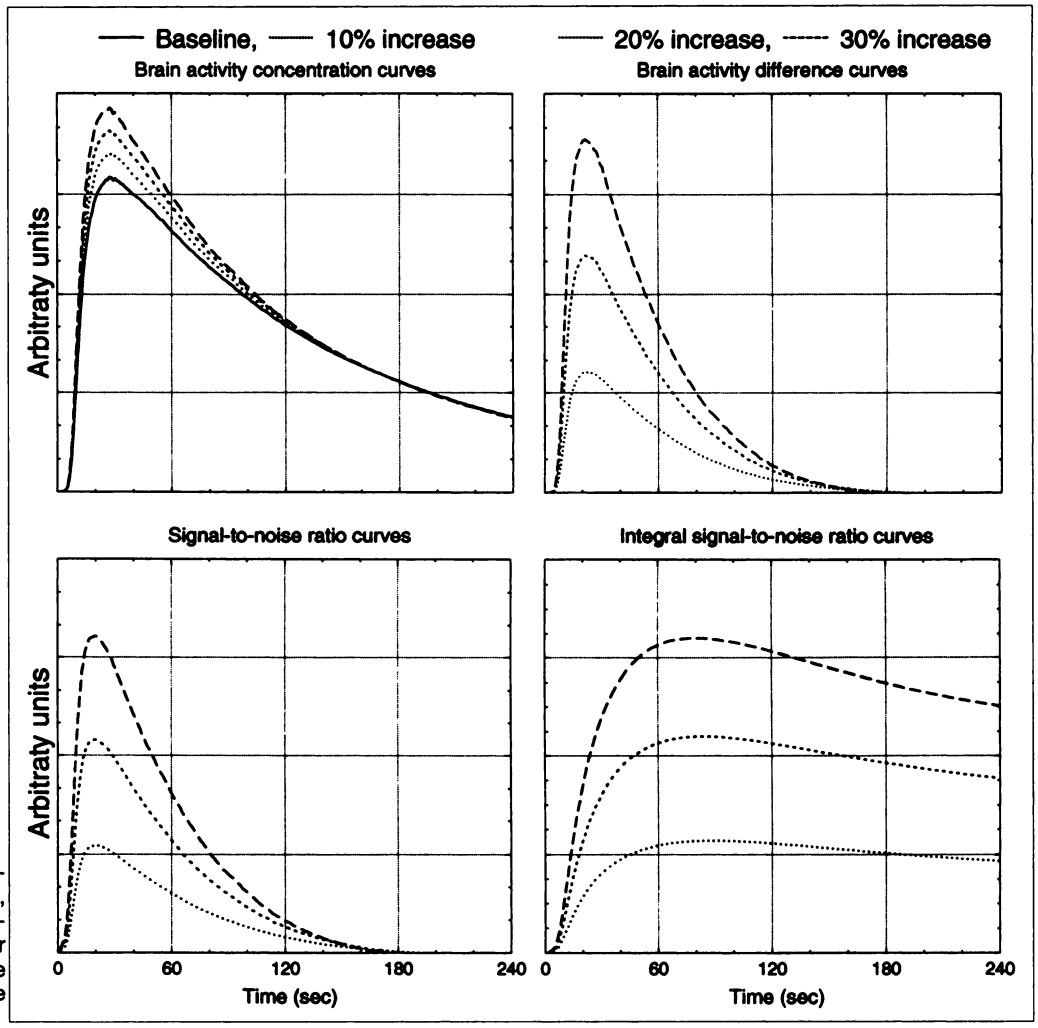

FIGURE 1. Examples of non-decay-corrected time-activity curves, signal curves, S/N curves and integral S/N curves obtained from the simulations. Gray matter flow of 70 ml/(min · 100 ml) and white matter flow of 17.5 ml/(min · 100 ml) were used to generate the curves.

Experiments

Examples of a scanner counting rate curve together with the resulting weights for the 15 frames are shown in Figure 3. Note how the frames around the peak of activity are given a high weight, and how the weights progressively diminish after the peak.

The S/N ratios obtained for straight and weighted summation for different summation times are presented in Table 1 and Figure 4. Table 1 demonstrates how the S/N ratio is significantly better for weighted than for straight summation when summation length exceeds 60 sec. More importantly, the highest S/N ratio obtained for weighted summation (summation time 100 sec) is significantly better ($p = 0.0023$, paired t-test) than the highest S/N ratio obtained for straight summation (summation time 60 sec). Note also the excellent agreement between simulated and experimental data evident in Figure 4. The magnitude of the improvement in S/N ratio is 6.3% for the experimental data.

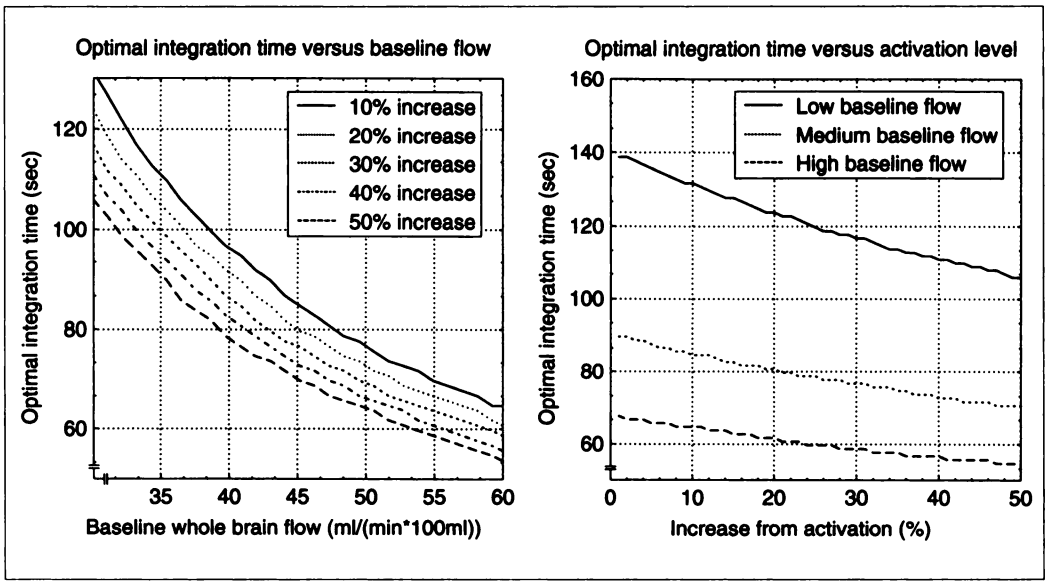

FIGURE 2. (Left) Optimal integration time for straight summation compared with baseline whole-brain blood flow. (Right) Dependence of activation level is shown. The jagged appearance of the curve is due to the fact that optimal integration time was evaluated with a granularity of 1 sec.

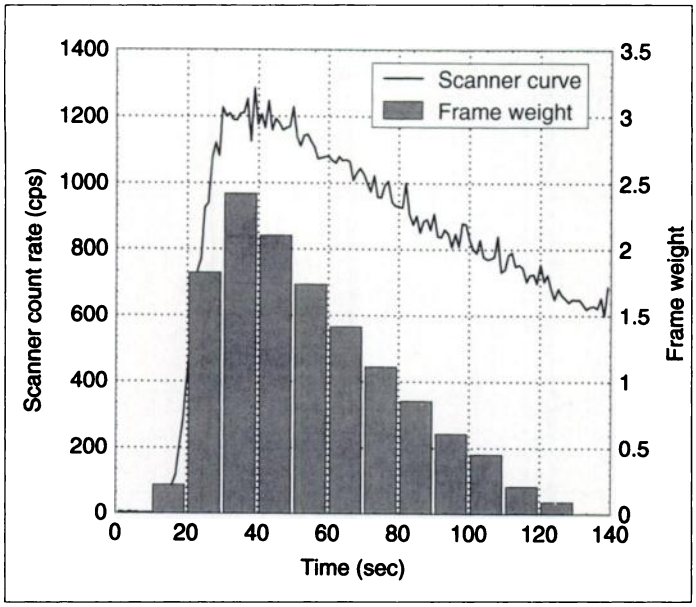

FIGURE 3. Examples of non-decay-corrected scanner curve and weights to be applied to each frame for one study participant.

The computational overhead imposed by the suggested method amounted to approximately 1 min per study (15 frames). This time consisted mainly of disk I/O and will hence depend strongly on the performance of the disks. Processing time will have a strong relationship to the size of the projection data and would hence increase a factor 5–10 for three-dimensional data.

DISCUSSION

By performing a weighted rather than a straight summation of $H_2{}^{15}O$ data, a significant increase in S/N ratio for activation studies may be achieved. This method does not involve manipulation of the experimental protocol or increase its invasiveness. Hence, it would be applicable in any type of perturbation that alter regional cerebral blood flow. Furthermore, in contrast to the situation for switched protocols (*9,10*), the blood flow is kept constant throughout the experiment. Thus, it may without reservation be combined with a quantitative analysis because the assumption of constant flow throughout the examination is not violated.

The S/N curve was chosen as a weight function for empirical reasons. Simulations were performed with a number of candidate functions, and the signal-to-noise ratio curve was the one that produced the highest S/N ratios. It was also the only one that yielded a plateau in the S/N ratio curve.

TABLE 1
S/N Ratios for Weighted and Straight Summation

Summation time (sec)	S/N ratio (Straight summation)	S/N ratio (Weighted summation)	p level (paired t-test)
40	2.92	2.87	0.38
60	2.98	3.04	0.23
80	2.96	3.09	0.0052*
100	2.86	3.17	0.0016*
120	2.78	3.15	0.00037*

The S/N ratio gain for the experimental data is almost identical to that predicted by the simulations. This is somewhat surprising as the estimate of whole-brain blood flow is bound to be associated with some uncertainty and thus also the estimated signal curve. This may be explained by two counteracting influences: First, the loss of gain caused by errors in the estimation of the signal curve and second, the addition in gain that comes from applying the method to a group of subjects. This is due to the interindividual variation in optimal summation time for straight summation, meaning that the peak S/N value will occur at different times for different individuals. This is evident when looking at the experimental data for each individual (data not shown), indicating that optimal S/N time is almost evenly distributed between 40 and 120 sec for straight summation, while optimal S/N ratio was obtained for 100 to 120 sec summation time in all subjects but one when performing weighted summation. Thus, when averaging over all subjects for each summation time, peak values will not add up when performing a straight summation but will in the case of a weighted summation.

The exact appearance of the weight curve will depend on the estimated global blood flow level, and also to a smaller extent on the level of activation that is chosen when calculating the signal curve. Thus, the activation level should be chosen so that it corresponds to the lowest level activation that can possibly be detected from the material at hand. The value of 20% used in the experimental part of this article was chosen rather arbitrarily, since it is a level of activation typically found for primary sensory responses (*1,26*). It should be noted that, regardless of the actual magnitude of the activation, there will

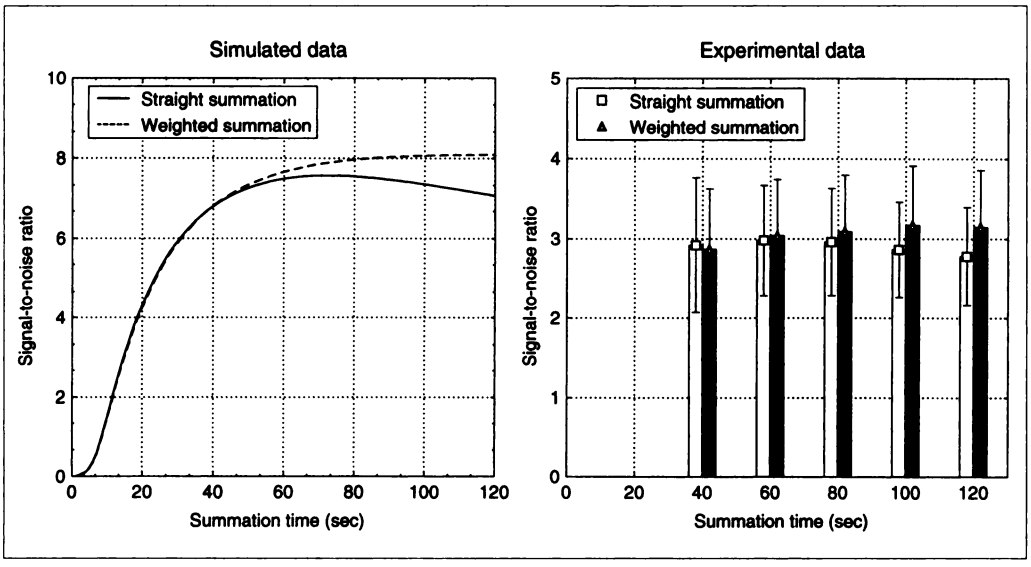

FIGURE 4. Comparison between straight and weighted summation, demonstrating the resulting S/N gains. Simulated data are shown on the left and experimental data on the right. A whole-brain flow of 45 ml/(min × 100 ml) and a 20% activation were used when generating the simulated curve. The large s.d. error bars for the experimental data are explained by a large inter-individual spread in S/N ratio.

be a gain in S/N ratio with the proposed method. This gain, however, will be maximized when there is correspondence between the assumed and the actual activation.

The S/N gain is smaller compared to that achieved by both the single-switched and the double-switched protocols (*10*). Some objections, however, may be raised against the use of switched protocols. For many activation studies, the baseline is not equal to the resting state but rather involves a task of its own. The design of activation studies involves designing tasks so that they differ only with respect to the mental process that one wishes to study. A baseline task may, for example, involve the completion of words from three letter word stems, in which no stem may be completed to form a word from a previously shown list of words, whereas a memory task may involve the same completion of words where some of the stems may be completed to form words from the list (*27*). The effects in terms of mental processing of performing a double switch on a protocol of this kind can hardly be foreseen and are likely not to be limited to switching on and off explicit memory retrieval. This type of concern is discussed by Cherry et al. (*10*), and they suggest that switching should be used primarily for studies of primary sensory input or simple motor tasks.

The approach suggested in this article is inspired primarily by the work of Volkow et al. (*9*) and Cherry et al. (*10*), using the known kinetics of $H_2{}^{15}O$ in the brain to increase the S/N ratio. It is also related to work aimed at clarifying the sensitivity of the total sum images to short transient blood flow increases at different times after start of injection of tracer (*28*). In contrast to the present method, they use the derivative of the scanner curve as a weight function, and they do not utilize the weight function to increase the S/N ratio, but rather to weight the entire sum image before inter-scan correlational analysis. Weighting of $H_2{}^{15}O$ data has also been used previously to maximize the S/N ratio in quantitative flow maps calculated with the integrated projection method (*18*). It is interesting to note the similarities of the weight curves obtained in the present paper to those obtained by Carson et al. (*18*) using a completely different strategy.

The gain achieved with the present method is by no means dramatic. It does, however, equal that obtained by injecting all subjects with 13% more activity. This is provided that there are no differential deadtime losses, which is rarely the case. Thus, the gain in terms of equivalent injected activity is actually slightly higher. It should also be viewed in the context of the newly revised figures for whole-body dose equivalents after injection of $H_2{}^{15}O$ (*29*), significantly lowering the amounts of radioactive water that may be administered to a healthy volunteer. The amount of information that may be retrieved for a given absorbed dose should always be maximized (*30*). Because the method performs the weighted summation on the projection data, the method may also be used on septaless three-dimensional scanners without exceedingly large sacrifices in terms of processing time. The disk space requirements for the data acquisition will increase with a factor that equals the number of frames.

The handling of the singles described in the Methods section is not theoretically correct, and represent a simplification that was chosen to facilitate the implementation of the present method within an existing software system for data collection and reconstruction. The suggested simplification will yield adequate results as long as the injected dose is chosen such that deadtime losses are within reasonable limits (~10%). Since the present method is aimed at maximizing the information yield per absorbed dose unit, it would hardly be rational to at the same time accept S/N losses resulting from a substantial deadtime. The suggested method is likely to be used only in conjunction with sensible dose fractionation protocols (*31*).

Although the method involves no additional steps in the experimental phase, the implementation of the software that estimates whole-brain flow and evaluates a signal curve is not trivial. Preliminary data indicate that the method is relatively insensitive to the exact appearance of the weight curve, and that a standard weight curve could be evaluated and applied to all studies, thus simplifying the implementation of the method considerably. This hypothesis, however, requires validation which was not undertaken in preparation of this article.

CONCLUSION

Significant gains in S/N ratio for activation studies may be achieved by performing a weighted summation of the PET data. The method does not increase invasiveness or affect the experimental protocol and is applicable to study all types of cognitive tasks (pharmacological perturbations or physiological states) affecting regional cerebral blood flow.

REFERENCES

1. Fox PT, Raichle ME. Stimulus rate dependence of regional cerebral blood flow in human striate cortex demonstrated by positron emission tomography. *J Neurophysiol* 1984;51:1109–1121.
2. Friston KJ, Grasby PM, Frith CD, et al. The neurotransmitter basis of cognition: psychopharmacological activation studies using positron emission tomography. In: Chadwick D, Whelan J, eds. *Ciba foundation symposium 163: exploring brain functional anatomy with positron tomography*. West Sussex: John Wiley and Sons; 1991:76–87.
3. Drevets WC, Videen TO, Price JL, Preskorn SH, Carmichael ST, Raichle ME. A functional anatomy of unipolar depression. *J Neurosci* 1992;12:3628–3642.
4. Herscovitch P, Markham J, Raichle ME. Brain blood flow measured with intravenous $H_2{}^{15}O$. I. Theory and error analysis. *J Nucl Med* 1983;24:782–789.
5. Raichle ME, Martin WRW, Herscovitch P, Mintun MA, Markham J. Brain blood flow measured with intravenous $H_2{}^{15}O$. II. Implementation and validation. *J Nucl Med* 1983;24:790–798.
6. Fox PT, Mintun MA. Noninvasive functional brain mapping by change-distribution analysis of averaged PET images of $H_2{}^{15}O$ tissue activity. *J Nucl Med* 1989;30:141–149.
7. Mintun MA, Raichle ME, Quarles RP. Length of PET data acquisition inversly affects ability to detect focal areas of brain activation. *J Cereb Blood Flow Metab* 1989; 9(suppl 1):349.
8. Iida H, Kanno I, Miura S. Rapid measurement of cerebral blood flow with positron emission tomography. In: Chadwick D, Whelan J, eds. *Ciba foundation symposium 163: exploring brain functional anatomy with positron tomography*. West Sussex: John Wiley and Sons; 1991:23–37.
9. Volkow ND, Mullani NA, Gould LK, Adler SS, Gatley SJ. Sensitivity of measurements of regional brain activation with oxygen-15-water and PET to time of stimulation and period of image reconstruction. *J Nucl Med* 1991;32:58–61.
10. Cherry SR, Woods RP, Doshi NK, Banerjee PK, Mazziotta JC. Improved signal-to-noise in PET activation studies using switched paradigms. *J Nucl Med* 1995;36:307–314.
11. Weiller C, May A, Limmroth V, et al. Brain stem activation in spontaneous human migraine attacks. *Nature Medicine* 1995;1:658–660.
12. Woods RP, Cherry SR, Mazziotta JC. Rapid automated algorithm for aligning and reslicing PET images. *J Comput Assist Tomogr* 1992;16:620–633.
13. Andersson JLR. A rapid and accurate method to realign PET scans utilizing image edge information. *J Nucl Med* 1995;36:657–669.
14. Friston KJ. Statistical parametric mapping. In: Thatcher RW, Hallet M, Zeffiro T, John ER, Huerta M, eds. *Functional neuroimaging: technical foundations*. San Diego: Academic Press; 1994:79–93.
15. Worsley KJ, Evans AC, Marret S, Neelin P. A three-dimensional statistical analysis for CBF activation studies in human brain. *J Cereb Blood Flow Metab* 1992;12:900–918.
16. Kety S. The theory and applications of the exchange of inert gas at the lungs and tissues. *Pharmacol Rev* 1951;3:1–41.
17. Meyer E. Simultaneous correction for tracer arrival delay and dispersion in CBF measurements by the $H_2{}^{15}O$ autoradiographic method and dynamic PET. *J Nucl Med* 1989;30:1069–1078.
18. Carson RE, Huang SC, Green MV. Weighted integration method for local cerebral blood flow measurements with positron emission tomography. *J Cereb Blood Flow Metab* 1986;6:245–258.
19. Eriksson L, Holte S, Bohm C, Kesselberg M, Hovander B. Automated blood sampling systems for positron emission tomography. *IEEE Trans Nucl Sci* 1988;35:703–704.
20. Herscovitch P, Raichle M. What is the correct value for the brain-blood partition coefficient for water? *J Cereb Blood Flow Metab* 1985;5:65–69.
21. Holte S, Eriksson L, Dahlbom M. A preliminary evaluation of the Scanditronix PC 2048–15B brain scanner. *Eur J Nucl Med* 1989;15:719–721.
22. Rowan JO, Harper AM. Measurement of cerebral blood flow in man. In: Mathie RT, ed. *Blood flow measurement in man*. Castle House Publications Ltd., Kent 1982;109–119.
23. Kanno I, Iida H, Miura S, et al. A system for cerebral blood flow measurement using

an $H_2{}^{15}O$ autoradiographic method and positron emission tomography. *J Cereb Blood Flow Metab* 1987;7:143–153.
24. Bergström M, Eriksson L, Bohm C, Blomqvist G, Litton J. Correction for scattered radiation in a ring detector positron camera by integral transformations of the projections. *J Comput Assist Tomogr* 1983;7:42–50.
25. Andersson JLR, Vagnhammar BE, Schneider H. Accurate attenuation correction despite movement during PET imaging. *J Nucl Med* 1995;36:670–678.
26. Fox PT, Burton H, Raichle ME. Mapping human somatosensory cortex with positron emission tomography. *J Neurosurg* 1987;67:34–43.
27. Squire LR, Ojemann JG, Miezin FM, Petersen SE, Videen TO, Raichle ME. Activation of the hippocampus in normal humans: a funtional anatomical study of memory. *Proc Natl Acad Sci USA* 1992;89:1837–1841.
28. Silbersweig DA, Stern E, Schnorr L, et al. Imaging transient, randomly occurring neurophysiological events in single subjects with positron emission tomography: an event related count rate correlational analysis. *J Cereb Blood Flow Metab* 1994;14: 771–782.
29. Smith T, Tong C, Lammertsma A, et al. Dosimetry of intravenously administered oxygen-15-labeled water in man: a model based on experimental human data from 21 subjects. *Eur J Nucl Med* 1994;21:1126–1134.
30. Ham HR. Do we really care about absorbed radiation dose? [Letter]. *Eur J Nucl Med* 1994;21:696–697.
31. Cherry SR, Woods RP, Hoffman EJ, Mazziotta JC. Improved detection of focal cerebral blood flow changes using three-dimensional positron emission tomography. *J Cereb Blood Flow Metab* 1993;13:630–638.

(continued from page 7A)

FIRST IMPRESSIONS

Hot Nose on Cerebral Perfusion Images

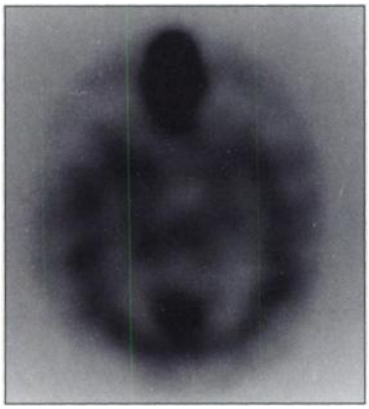

Figure 1.

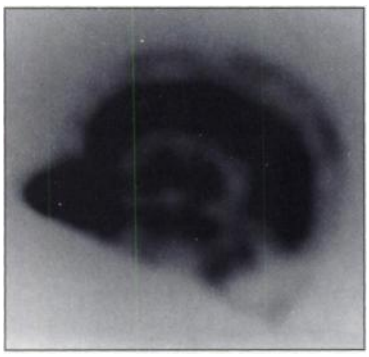

Figure 2.

PURPOSE

A 59-yr-old woman with two aneurysms of the left internal carotid artery underwent a brain scan with balloon occlusion of the affected carotid artery. She was crying during and after the balloon occlusion, frequently blowing and wiping her nose with a handkerchief. No significant perfusion abnormalities of the brain were present. Intense activity is seen in the nose (Figs. 1 and 2). Subsequently, the handkerchief demonstrated accumulation of ^{99m}Tc-HMPAO.

Lacrimal gland uptake of ^{99m}Tc-HMPAO is present in 11% of patients. The lack of lacrimal gland activity in this patient may be due to increased tear production and exponential washout from these glands.

TRACER

Technetium-99m-HMPAO, 30 mCi

ROUTE OF ADMINISTRATION

Intravenous

TIME AFTER INJECTION

30 minutes

INSTRUMENTATION

ADAC Dual-Head Vertex SPECT camera; Genesys computer system (64 × 64 matrix, 128 projections with 360° rotation); FOV mask center 38; time per step, 30 sec

CONTRIBUTORS

Vincent Robinson and George Burke, Medical College of Georgia, Augusta, Georgia